Improvement of the contrast-to-noise ratio in pulse-phase thermography by frequency dependent windowing

by U. Netzelmann[1] and D. Müller[2]

[1]Fraunhofer Institute for Non-Destructive Testing IZFP, Campus E3 1, 66123 Saarbrücken, Germany, *udo.netzelmann@izfp.fraunhofer.de*

[2]Hochschule für Technik und Wirtschaft des Saarlandes, htw saar, Goebenstr. 40, 66117 Saarbrücken, Germany, *david.mueller@izfp.fraunhofer.de*

Abstract

Two modified algorithms for pulsed phase thermography were defined. The principle is to mask out parts of the thermal signal that only add noise but no significant information. The algorithms were tested on synthetic signals from a circular hidden defect and experimentally by flash excited thermography on a steel and a polymer sample. A significant improvement of the contrast-to-noise ratio of defects was obtained for higher analysis frequencies.

1. Introduction

Pulsed phase thermography (PPT) [1] is a frequently used method to process thermographic image sequences. It is usually applied in active thermography, when pulsed excitation is generated by a flash or by a short pulse from a laser or an electromagnetic inductor. A thermographic image sequence of a certain length is recorded, starting with the beginning of the pulsed excitation. Then, for each pixel in the image, the time dependence of the thermal signal is Fourier transformed over the length of the sequence. A complex signal in the frequency domain is obtained for a set of frequencies and an amplitude and a phase signal will be calculated for every frequency. From the amplitude and phase values of all pixels, amplitude and phase images are constructed.

The strength of the phase images is that they ideally only represent time-dependent effects and suppress multiplicative influences in the signal, like inhomogeneous illumination and heating, or local variations of the infrared emissivity. In addition, it has been shown that the phase signal usually allows one the obtain information from larger depth than the amplitude signal. A major advantage of PPT is that it uses not only information from a single recorded frame, but from all frames in the recorded image sequence, thereby leading to a significant improvement of the contrast-to-noise ratio (CNR) obtained from defects. Using low as well as high analysis frequencies obtained by the PPT, from a single measurement one can detect deep defects (at low frequencies) and very shallow defects (at higher analysis frequencies). This is similar to what is called thermal wave depth profiling, but obtained by a broad-band pulsed excitation.

Classical PPT handles all parts of the recorded IR image sequence in a similar way, the early parts as well as the late parts in the sequence. For periodic excitation (like in lock-in thermography) this is very useful, as the excitation extends over the whole recorded sequence. Then, the thermal signal rises proportional to the number of modulation periods in the sequence, whereas the noise only accumulates with the square root of the recording time. In total, the signal-to-noise will improve with the length of the recorded sequence [2]. However, it is different in the case of a typical thermal response following pulsed excitation in reflection arrangement (heated surface on the camera side). Temperature changes with time will be high at the early time of the recorded signal, but slower at later time. This is a consequence of the physics of the diffusion and renders it impossible that suddenly a rapid change in the signal may occur at a longer time. At longer times, there is no additional contribution to the higher frequency components of the thermal signal, but only an accumulation of the noise.

One previous attempt to improve the signal/noise obtained from PPT was to combine it with the thermographic signal reconstruction (TSR) [3]. In his work on PPT, Ibarra Castanedo pointed out that for high thermal conductivity materials the number of frames recorded can be reduced without loss of information [4]. In the focus were the Fourier transform aspects of PPT. From data of D´Accardi et al. [5] focused on comparisons of different pre-processing techniques it can be seen that the contrast-to-noise of hidden defects in PPT increases when the recorded length is reduced. PPT has been compared with other techniques like TSR, principal component thermography, normalized thermal contrast or orthogonal polynomial decomposition, e. g. [6]. Marani et al. used preprocessing by a finite-impulse response filter with fixed filter parameters to improve classification of defects [7]. The effect of truncation of the recorded thermography data before and after the heating pulse before applying PPT has been studied by Waugh et al. [8]. Although not mentioned explicitly, their data allow one to deduce that the contrast-to-noise ratio of defects will increase with truncation of the late parts of the recorded sequence. In [9], there is an analysis of the frequency dependent phase noise in PPT. The authors showed that the phase noise increases with increasing analysis frequency.

In this contribution it will be demonstrated that by taking profit of the above mentioned property of thermal response signals after pulsed excitation, a modified PPT can be defined, that improves the contrast-to-noise ratios (CNR) at the higher analysis frequencies significantly although using the same recorded image sequence. After a short review of the classical PPT (section 2), a modified PPT (PPT1) will be defined (section 3). PPT1 will need more processing time.

Therefore, another modified algorithm, PPT2, is suggested in section 4, which does not increase processing time very much compared to classical PPT. Both algorithms will be analysed using artificial thermal data from an analytical model with added noise (section 5). Finally, all three algorithms are applied to experimental data and the improvements in CNR will be analysed along with the cost in computation time (section 6).

2. Classical pulsed phase thermography (PPT)

A thermographic image sequence consisting of N images recorded over a total time T will be analysed pixel by pixel. The time dependent signal $T(k \cdot T/N) = T_k$, $k=0…N-1$, will be transformed into the frequency domain by a discrete Fourier transform [1]:

$$F_n = \sum_{k=0}^{N-1} T_k e^{-2\pi ikn/N} = \mathrm{Re}_n + \mathrm{Im}_n \tag{1}$$

From the real and imaginary parts of the transform result for frequency number n, Re_n and Im_n, respectively, the amplitude A_n and the phase φ_n can be calculated:

$$A_n = \sqrt{\mathrm{Re}_n{}^2 + \mathrm{Im}_n{}^2} \qquad\qquad \varphi_n = \arctan\frac{\mathrm{Im}_n}{\mathrm{Re}_n} \tag{2}$$

Here, n is index of the frequency ($n=0,1,…,(N-1)$). After execution for all pixels, an amplitude and a phase image are generated for discrete, equally spaced frequencies

$$f_n = \frac{n}{T} \tag{3}$$

Usually, eq. 1 will be computed by using a fast Fourier transform (FFT) algorithm in order to speed up the calculation for all pixels of an image significantly. The computational load is of the order of N log N.
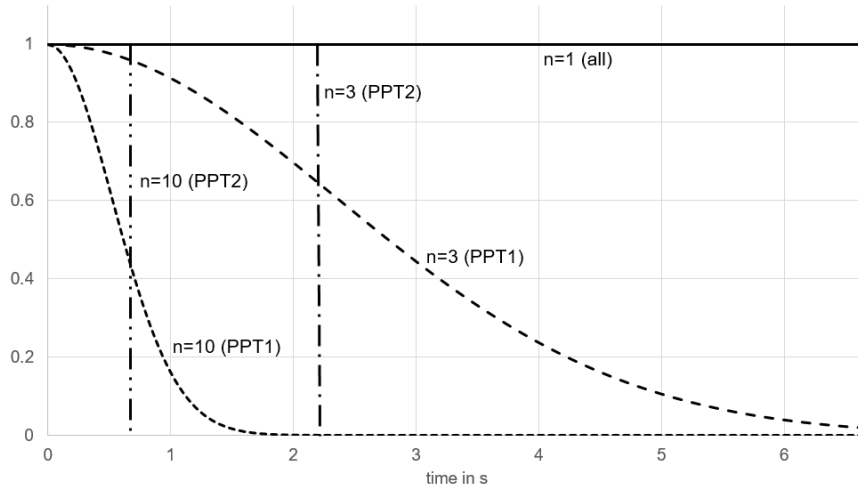

Fig. 1. Scheme of the window functions for the frequency numbers n=1, 3 and 10 used for the modified algorithms PPT1 and PPT2

3. Modified PPT calculation by discrete Fourier transform (PPT1)

In order to obtain the desired improvement of the contrast/noise ratio in the data in the frequency space, it is suggested to modify the PPT algorithm to PPT1 by a frequency dependent Gaussian window-function (figure 1):

$$F_n^{PPT1} = \sum_{k=0}^{N-1} \Delta T_k e^{-(\frac{k(n-1)}{N})^2} e^{-2\pi ikn/N} \tag{4}$$

Here, ΔT_k is the temperature change $T_k - T_0$ due to heating. The result for the frequency with index n=0 is usually not of interest in active thermography. It will be modified, but in any case yields a weighted average value over time. For the lowest useful analysis frequency with n=1, the window term is neutral. Here, the result will be the same as in PPT. The higher the frequency, the more of the signal at the end of the recorded sequence will be cut off, and only the early part (containing the higher frequency components) will contribute to the Fourier component. A disadvantage of PPT1 is the longer computation time. Due to the modification term, which itself depends on the summation index k, application of the

fast Fourier transform (FFT) algorithm is no longer possible and a discrete Fourier transform (DFT) is necessary. The computational load is increased to the order of N^2.

4. Modified PPT calculation using FFT (PPT2)

In order to avoid the disadvantage of the longer calculation times needed for PPT1, a second modification (PPT2) was implemented, that allows to use FFT algorithm. The idea of the PPT2 algorithm is to use for each analysis frequency only the first period of the sine/cosine kernel, by this cutting away the later parts of the recorded signal (figure 1). The length of the data set to be transformed is thereby reduced with increasing frequency n. For each transform result, only the first frequency after the zero frequency is considered. The calculation for PPT2 is given by eq. 5.

$$F_n^{PPT2} = \sum_{k=0}^{Round(N/n)-1} T_k e^{-2\pi i k / Round(N/n)} \qquad n>0 \qquad (5)$$

For the lowest analysis frequency (n=1), the result is identical to classical PPT. The computation of (5) can be performed using a FFT algorithm. Only one complex value is really used from each FFT. The total computation time is longer than for PPT, but faster than that of the DFT necessary for PPT1. The reasons are that FFT works very fast and that the length of the FFT data field to be transformed is rapidly decreasing with n. A disadvantage is, that due to the round function one may obtain the same F_n^{PPT2} values for different n, in particular for higher values of n. This leads to the stepped behavior in the amplitude and phase curves and reduces the actual spectral precision and resolution at the high frequencies.

5. Analytically simulated contrast from circular hidden defects

In order to test the algorithm on realistic simulated data, an approximative analytical solution from the signal of a circular defect with finite diameter D in an otherwise homogeneous plate was determined [10,11]. The thermal responses at a reference position and at a defect position were calculated. If one considers a homogeneous plate with thickness L heated homogeneously at t=0 by a delta pulse leading to an absorbed surface energy density of Q_0, the surface temperature change can be described as

$$\Delta T_r = \frac{Q_0}{\sqrt{\pi}\sqrt{\lambda \rho c}\sqrt{t}}\left[1 + \sum_{n=1}^{\infty} R_p^{\ n} e^{-\frac{(nL)^2}{\alpha t}}\right] \qquad (6)$$

Here, λ is the thermal conductivity, ρ the density and c the specific heat capacity, $\alpha = \lambda/(\rho c)$ is the thermal diffusivity of the material. R_p the thermal reflection coefficient at the back side of the plate. If parallel to the heated surface there is a circular defect with diameter D and in a depth of d under the heated surface, according to [6] the surface temperature change over the center of the defect can be approximated by [10]

$$\Delta T_d = \frac{Q_0}{\sqrt{\pi}\sqrt{\lambda \rho c}\sqrt{t}}\left[1 + \sum_{n=1}^{\infty} R_d^{\ n} e^{-\frac{(nd)^2}{\alpha t}} \cdot (1 - e^{-\frac{(D/2)^2}{4\alpha t}})\right] \qquad (7)$$

R_d the thermal reflection coefficient of the circular defect. Equation (8) considers the multiple reflections of the heat pulse between defect and surface and the lateral heat flow from the trapped heat over the defect. Signals as a function of time were calculated with material parameters in Table 1 using a Mathematica program based on eqs. (6) and (7). A plot of the artificial signals over a time of 6.7s with an assumed frame rate of 150Hz is shown in figure 2. For the application of the PPT algorithms, the analytical data were digitized in N=1000 samples over the recording time.

Table 1: *Parameters used for the calculation of the surface temperature*

Parameters	Symbol	Value
Heat source input	Q_0	10000J/(m^2)
Defect depth	d	500µm
Defect diameter	D	10mm
Plate thickness	L	5mm
Thermal conductivity	λ	44.5W/(mK)
Specific heat capacity	c	475J/(kgK)
Density	ρ	7850kg/(m^3)
Thermal reflection factor	R_p, R_d	1

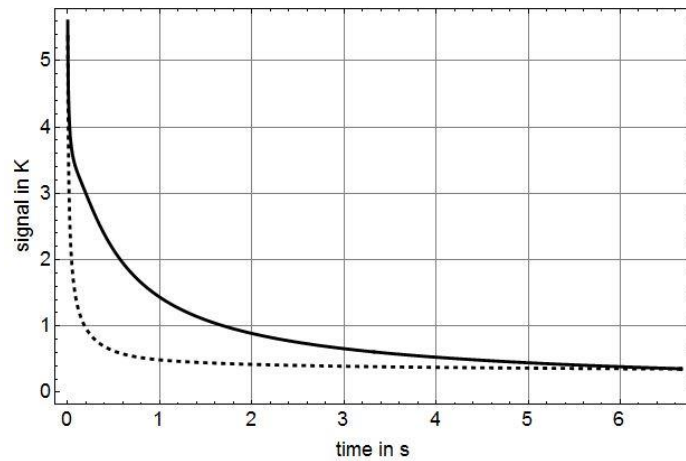***Fig. 2.*** *Calculated thermal decay curve ΔT$_d$(t) at a point central over a defect (solid line) and ΔT$_r$(t) over a reference point (dashed line)*

For the following investigations, random noise of 0.01 K was added both to ΔTd(t) and ΔTr(t).

Classical PPT and the PPT1 and PPT2 algorithms were applied for the defect and the reference signals. Then, the absolute phase contrast φ_d-φ_r between defect and reference was calculated and is shown in figure 3.
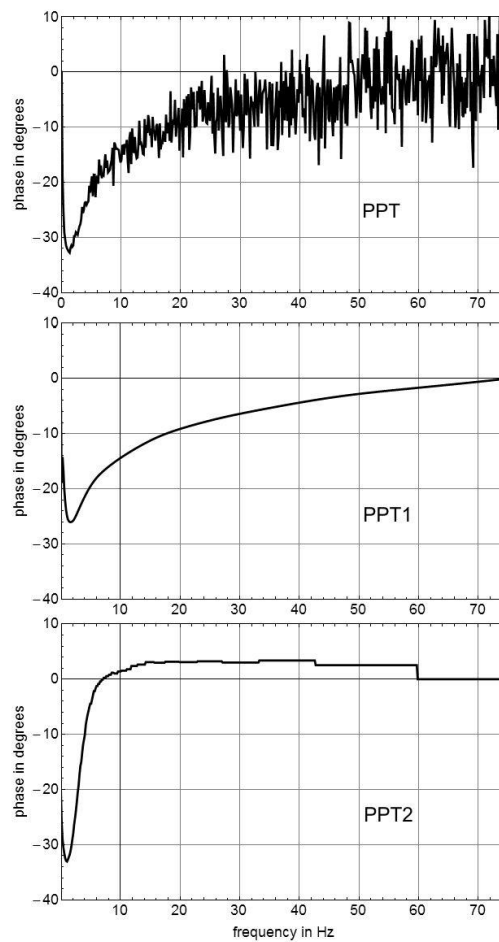

Fig. 3. *Simulated phase contrast as a function of frequency over a flat bottom hole obtained from classical PPT (top), PPT1 (middle) and PPT2 (bottom)*

The suppression on noise is clearly visible in the data and extremely high at high analysis frequencies up to the Nyquist frequency (here 75 Hz). At low frequencies below 10Hz, the absolute phase contrast of PPT1 is somewhat reduced compared to PPT, but the contrast/noise ratio is still higher.

For PPT2, the phase minimum at a frequency of about 1Hz is reproduced well in position and its value. At higher frequencies, there is a strong deviation of the phase contrast. At about 7Hz, there even is an inversion of the contrast, which does not occur in PPT. Nevertheless, the noise level is clearly reduced at the higher frequencies. The steps in the phase contrast curve from PPT2 are due to the round function. For the present parameters, meaningful data can be achieved up to about 50Hz.

6. Experiments

Experiments were performed in order to verify the simulated results. Test blocks were made of ferritic steel and polyvinylchloride (PVC) with dimensions of 100 mm x 100 mm and 5 mm thickness. They contained back-side flat bottom holes as sketched in figure 4. The front side was blackened by a thin layer of black paint.
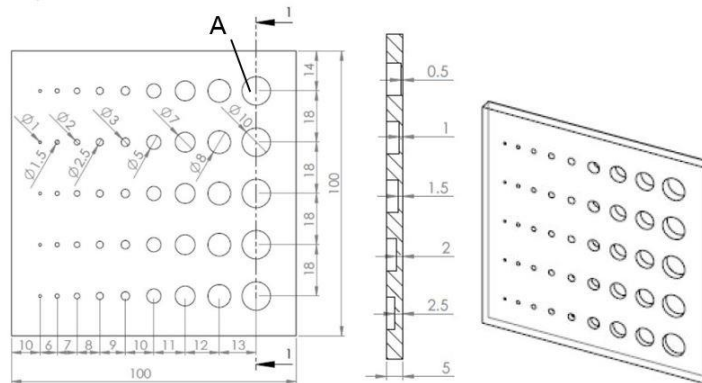

Fig. 4. Technical drawing of the test sample (back-side view). Dimensions in mm [12]

The samples were tested from the front side by flash thermography using two flashes each operated at 3.2kJ energy. This was intentionally at half of their maximum output, as a sufficient level of noise should be in the experimental data. As a second effect, detector saturation during flash heating was avoided. The steel sample was imaged using a FLIR SC5200 camera at 150 frames/s and 600µs integration time. Some frames before the flash were recorded for background subtraction and 1000 frames were recorded during and after the flash. For the steel sample, a cooling curve on a central pixel over the flat bottom hole A (figure 4) with 10mm diameter and 0.5mm coverage (figure 4) and a curve on a reference point far from the defects are shown in figure 5, to be compared with figure 2.
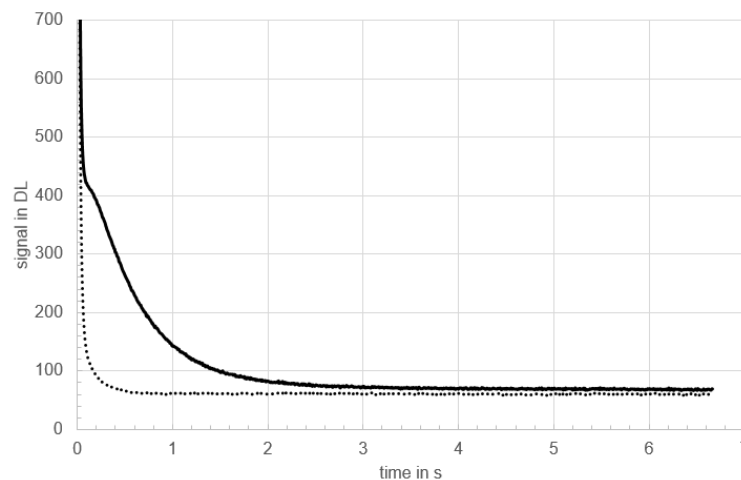

Fig. 5. Experimental thermal decay curves of the signal change in digital levels (DL) at a point central over a defect (solid line) and over a reference point (dashed line)

Differences between the experimental and the simulation results may be due to the uncertainty of the exact thermal diffusivity of the steel. Furthermore, as the approximation in eq. (7) underestimates the role of 3D thermal diffusion at longer times after excitation, the defect contrast decays faster in the experiment than in the simulation.

The image sequences were processed by PPT, PPT1 and PPT2 based on eqs. (1), (4) and (7) using a Matlab software. The frequency dependent amplitude and phase curves were determined on a central pixel over the flat bottom hole A (figure 4). The relative amplitude contrast A_d/A_r and the absolute phase contrast $\varphi_d-\varphi_r$ of the defect were then determined as a function of the analysis frequency. Figure 6 shows the relative amplitude contrast and figure 7 the absolute phase contrast.
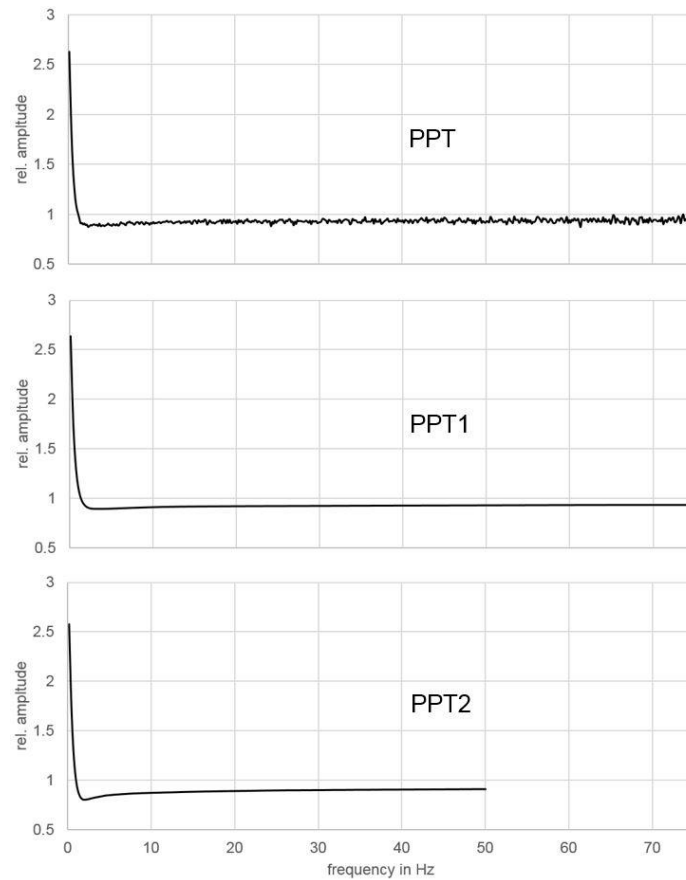

Fig. 6. *Experimentally determined relative amplitude contrast of a flat bottom hole in steel as a function of the analysis frequency for PPT (top) PPT1 (middle) and PPT2 (bottom)*

The relative amplitude curves for all variants of PPT in figure 6 are very similar. PPT exhibits more noise than PPT1 and PPT2. The experimental phase contrast (figure 7) clearly shows noise with a level increasing with frequency. Again, for PPT1 and PPT2 there is much less noise in the curves than for PPT. As usual for hidden defects with lower effusivity, a phase minimum is obtained at a certain frequency. PPT2 shows a sign change of the absolute phase contrast at 2.7Hz which is not obtained in PPT and PPT1.
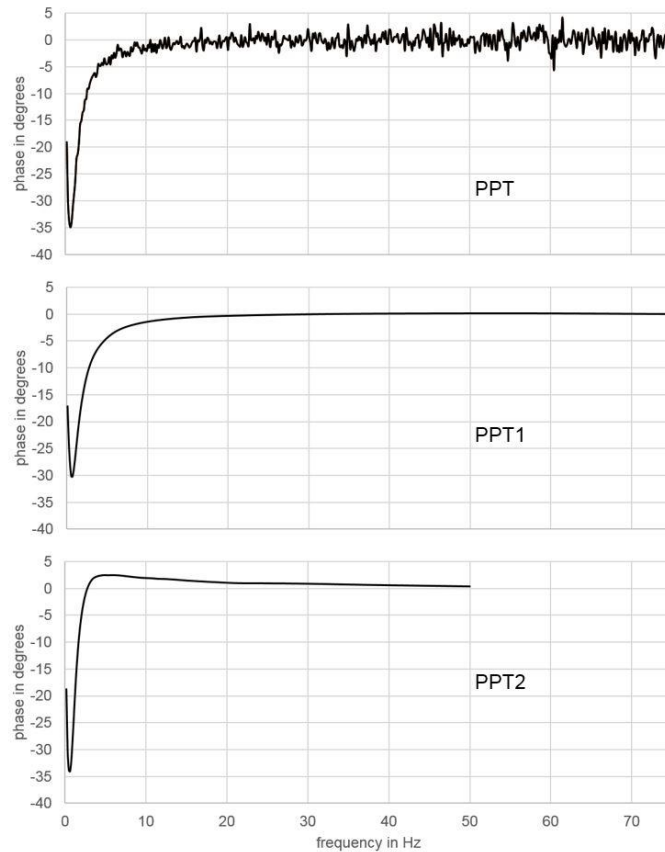
Fig. 7. *Experimentally determined absolute phase contrast of a flat bottom hole in steel as a function of the analysis frequency for PPT (top) PPT1 (middle) and PPT2 (bottom)*

In figure 8, phase images resulting from PPT, PPT1 and PPT2 at two different frequencies are shown for comparison. At a given frequency, the phase span displayed is the same for all variants of PPT. The flat bottom hole A appears in the upper right corner both in figures 4 and 8, but the sample view is mirrored and rotated. Some parameters extracted from the experimental data are shown in Table 2. The absolute of the phase contrast-to-noise ratio (CNR) is listed.

Table 2: *Parameters from experimental results for defect A in the steel sample obtained with the three preprocessing techniques*

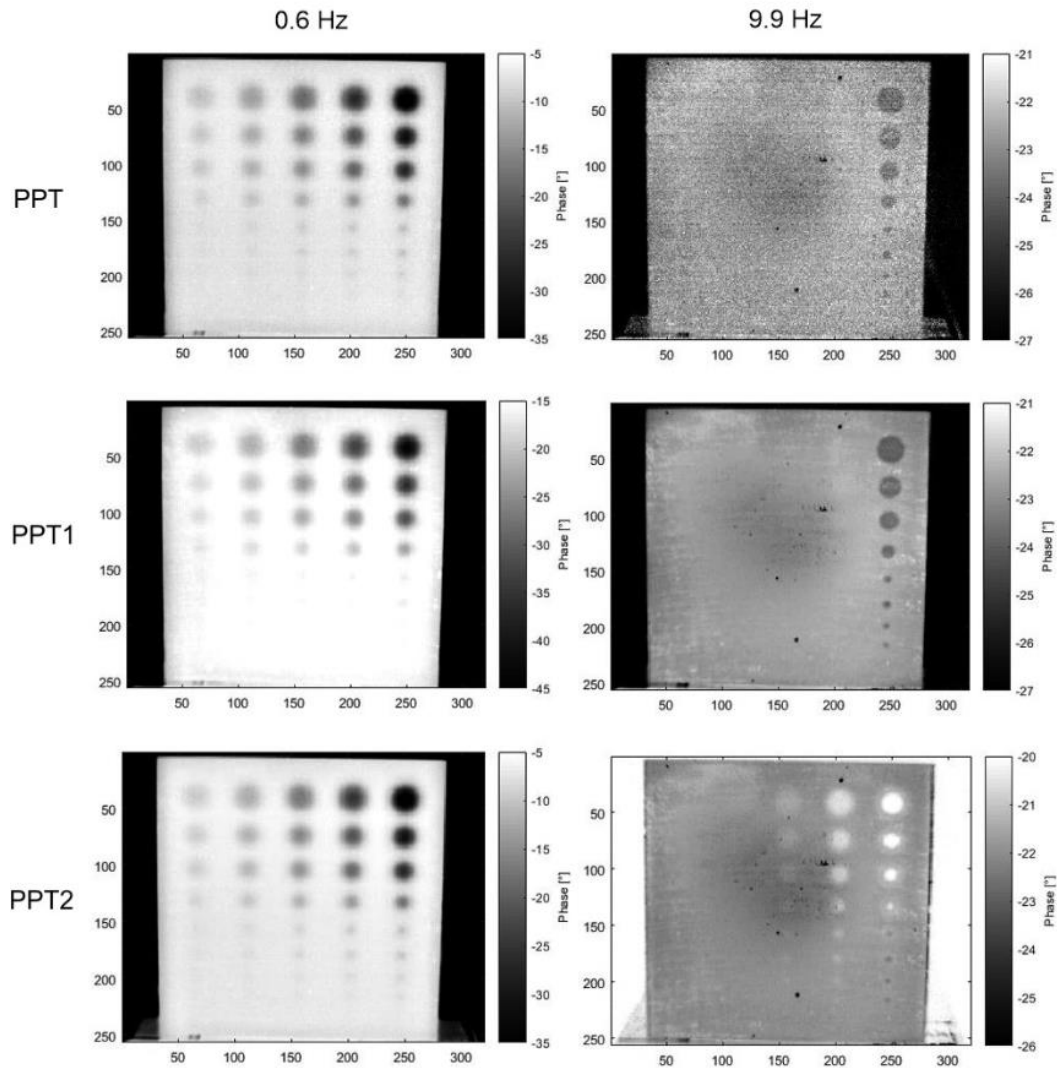| Parameters	PPT	PPT1	PPT2
Frequency of the phase minimum	0.6Hz	0.71Hz	0.54Hz
Value of the phase minimum	-35.0°	-30.5°	-34.4°
Frequency, where the relative amplitude is one	1.28Hz	1.42Hz	0.95Hz
Minimum of the relative amplitude	0.85	0.85	0.80
CNR at 0.6Hz	82.8	134.4	102.0
CNR at 9.9Hz	3.21	19.3	26.3
CNR at 20.1Hz	-	4.4	15.5
Computation time	3.7s	12.6s	9.3s

Fig. 8. *Thermographic phase images from the steel sample at 0.6Hz (left column) and at 9.9Hz (right column).*
Top row: Classical PPT, middle row: PPT1, bottom row: PPT2

At a frequency of 0.6Hz (close to the phase minimum) the images are looking quite similar, although PPT is somewhat noisier. At 9.9Hz, the PPT image looks much noisier than the images generated by the modified versions. In the PPT2 image, two columns of defects with larger coverage become visible. However, there is also the inversion of the contrast as mentioned above.

There are changes in the value of the phase minimum and its position in frequency. For 0.6Hz (close to the phase minimum), there is an improvement in CNR for PPT1 and PPT2. At 9.9Hz (10Hz for PPT2), the CNR is significantly improved both for PPT1 and PPT2. At 20.1Hz (21.43Hz for PPT2), defect A was not detectable in the PPT image, but it was still detectable with sufficient CNR by PPT1 and PPT2.

Furthermore, in Table 2 the computation times are listed for a sequence of 1000 images with 320 x 256 pixels under Matlab running on an Intel Xeon CPU E5-2665 @ 2.4GHz (16 cores), and 128 GB RAM. In this special case, PPT is the fastest algorithm. PPT2 is slower by a factor of 2.5 and PPT1 by a factor of 3.4, respectively.
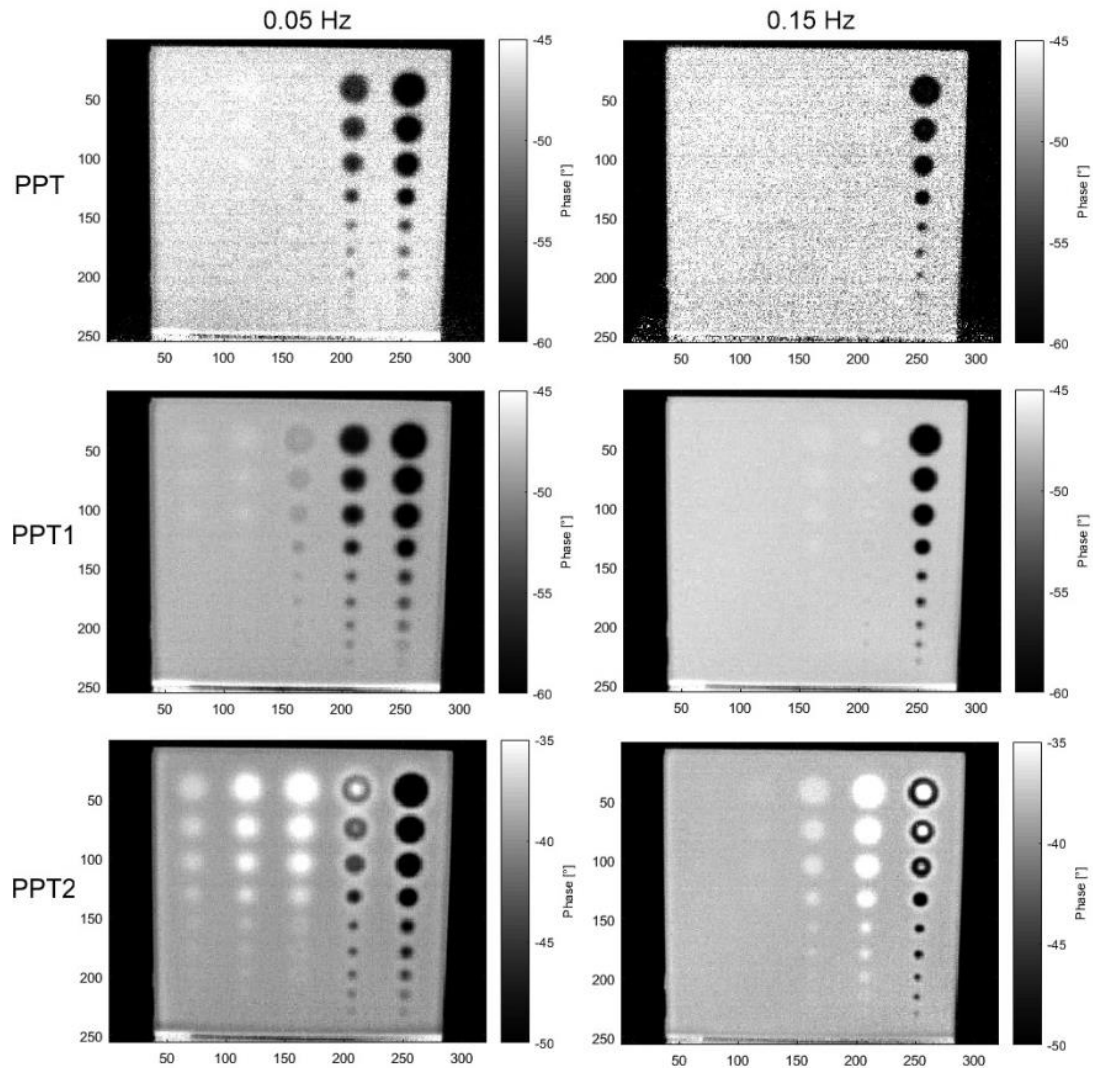
. 9. Thermographic phase images from the polymer sample at 0.05 Hz (left column) and at 0.15 Hz (right column). Top row: Classical PPT, middle row: PPT1, bottom row: PPT2

For the polymer sample, the measurement parameters were the same, except the frame rate, which was reduced to 2 frames/s due to the much lower thermal diffusivity of the polymer. Phase images at selected frequencies of 0.05Hz and 0.15Hz (0.154Hz for PPT2) are shown in figure 9.

Some parameters extracted from the experimental data on the polymer sample are shown in Table 3.

Table 3: *Parameters from experimental results for defect A in the polymer sample obtained with the three preprocessing techniques*

Parameters	PPT	PPT1	PPT2
Frequency of the phase minimum	0.052Hz	0.048Hz	0.040Hz
Value of the phase minimum	-31.6°	-27.3°	-37.6°
Frequency, where the relative amplitude is one	0.16Hz	0.29Hz	0.04Hz
Minimum of the relative amplitude	0.97	0.97	0,44
CNR at 0.05Hz	20.3	94.2	115
CNR at 0.15Hz	6.0	78.5	55.0

CNR at 0.45Hz	-	3.1	24.4
Computation time	4.4s	12.8s	7.9s

The results for PVC are qualitatively similar to that of steel. The PPT2 data of the frequency and the value of the phase minimum deviate more from PPT than for the steel sample. But again, generally a significant improvement in CNR can be found at the higher analysis frequencies for PPT2 and PPT1.

7. Discussion

The noise added in the simulation is white noise, whereas the noise power spectrum of typical IR cameras is dominant at lower frequencies and may even show some resonance peaks.

The variations of the position of the phase minimum and its depth are due to the effect of the truncation windows used in the PPT1 and PPT2 algorithms. This has been discussed in detail in [4]. Even classical PPT is affected by leakage effects due to the finite recording length and by frequency dependent phase changes due to the finite length of the excitation pulse. A disadvantage of PPT2 is the change of the sign of the contrast, which may hide certain defects at this frequency.

It should be pointed out that the PPT1 algorithm requires a background subtraction before application. Otherwise the window function will cause significant distortions of the phase.

Both modifications will suppress the effect of uneven heating as classical PPT does, as real and imaginary part are affected by the same factor.

8. Conclusion

The present simulations and experiments have shown that the two modified PPT algorithms defined can significantly improve the contrast-to-noise ratio of defects compared to classical PPT, when higher analysis frequencies are considered. They will have advantages, if defects can be expected in different unknown depth. The phase as a function of the analysis frequency will have deviations from classical PPT, which may have negative effects on quantitative defect characterization. Nevertheless, due to the reduced noise defects were revealed at higher frequencies that were not detected by classical PPT. At least a fast screening for defects should be facilitated. The somewhat increased calculation times appear to be acceptable in many cases.

REFERENCES

[1] Maldague X., Marinetti S., Pulse phase infrared thermography, J. Appl. Phys. 79, 1996, 2694-2898.
[2] Breitenstein O., Langenkamp M., "Lock-in Thermography", Springer, Berlin, 2003.
[3] Maldague X., Galmiche F., Ziadi A., Advances in pulse phase thermography, Infrared Phys. and Techn. 43, 2002, 175-181.
[4] Ibarra Castanedo C., Quantitative subsurface defect evaluation by pulsed phase thermography: depth retrieval with the phase, PhD thesis, (Universite Laval, Quebec 2005).
[5] D´Accardi E., Palumbo D., Tamborrino R., Cavallo P., Galietti U., Pulsed Thermography: evaluation and quantitative analysis of defects through different post-processing algorithms, Quant. InfraRed Thermography Conference 2018, paper We.3.B.5.
[6] Avarez-Restrepo C., Benitez-Restrepo H., Tobon L., Characterization of defects of pulsed thermography inspections by orthogonal polynomial decomposition, NDT&E International 91, 2017, 9-21.
[7] Marani R., Palumbo D., Galietti U., Stella E., D´Orazio T., Enhancing defects characterization in pulsed thermography by noise reduction, NDT&E International 102, 2019, 226-233.
[8] Waugh R., Dulieu-Barton J., Simon Q., Defect detection using pulse phase thermography – repeatability and reliability of data, Key Engineering Materials 569-570, 2013, 1164-1169.
[9] Ishikawa M., Hatta H., Habuka Y., Fukui R., Utsunomiya S., Detecting deeper defects using pulse phase thermography, Infrared Physics & Technology 57, 2013, 42-49.
[10] Almond D., Pickering S., An analytical study of the pulsed detection limit, J. Appl. Phys. 111, 2012, 093510.
[11] Kalyanavalli V., Abilasha Ramadhas T., Sastikumar D., Long pulse thermography investigations of basalt fiber reinforced composite, NDT&E International 100, 2018, 84-91.
[12] Rubert K., Master-Thesis, htw Saar and Fraunhofer IZFP, 2018.